

# Finer sub-Planck structures and displacement sensitivity of $SU(1,1)$ circular states

Naeem Akhtar,<sup>1</sup> Jia-Xin Peng,<sup>2,\*</sup> Tariq Aziz,<sup>1</sup> Xiaosen Yang,<sup>3</sup> and Dong Wang<sup>1,†</sup>

<sup>1</sup>*School of Physics, Anhui University, Hefei 230601, China*

<sup>2</sup>*School of Physics and Technology, Nantong University, Nantong 226019, China*

<sup>3</sup>*Department of Physics, Jiangsu University, Zhenjiang, Jiangsu 212013, China*

(Dated: February 17, 2026)

Quantum states with sub-Planck features exhibit sensitivity to phase-space displacements beyond the standard quantum limit, making them useful for quantum metrology. In the context of the  $SU(1,1)$  group, sub-Planck features have been constructed through the superposition of four Perelomov coherent states on the hyperbolic plane (the  $SU(1,1)$  compass state). However, these structures differ in scale along different phase-space directions, resulting in nonuniform sensitivity enhancement. We overcome this limitation by constructing  $\bar{n}$ -component compass states, which are obtained by superposing  $\bar{n} \geq 6$   $SU(1,1)$  coherent states, with an even total number, evenly arranged along a circular path on the hyperbolic plane; that is, all components lie at the same distance from the origin and have equal angular spacing of  $\frac{2\pi}{\bar{n}}$ . These generalized  $SU(1,1)$  compass states generate circularly shaped sub-Planck features (isotropic sub-Planckness) and provide uniform enhancement in sensitivity to phase-space displacements. As the number of coherent states  $\bar{n}$  increases, these refinements progressively improve. While verified for  $\bar{n} = 16$   $SU(1,1)$  coherent states, the results remain valid for superpositions with arbitrarily large  $\bar{n}$  components.

## I. INTRODUCTION

The quantum uncertainty principle [1, 2], derived from commutator relations such as the position-momentum quadratures  $[\hat{x}, \hat{p}] = i\hbar$ , imposes a limit on the size of a phase-space structure. In the Wigner phase-space representation associated with the Heisenberg-Weyl (HW) symmetry [3], the product of uncertainties in position ( $\Delta x$ ) and momentum ( $\Delta p$ ) estimates the phase-space size of a feature, which satisfies the uncertainty relation  $\Delta x \Delta p \geq \frac{\hbar}{2}$ , implying that a phase-space feature cannot be smaller than the Planck scale ( $\hbar$ ). One might question the possibility of phase-space features smaller than the Planck scale (sub-Planck structures). While such sub-Planck features challenge the uncertainty principle and raise doubts about their physical implications, these traits appear to have tangible physical consequences. In simpler terms, they may exist [4–7], and are indeed physical [8], with their role being particularly crucial in quantum metrology [9–13].

Sub-Planck structures have been created from diverse quantum states, particularly within the HW group [14–19], with less attention given to analogs in other symmetry groups [20, 21]. The  $SU(1,1)$  group has shown considerable utility in quantum metrology [22–29], non-classical state generation [30–32], and two-photon phenomena [33, 34], to name a few. The superposition of four Perelomov  $SU(1,1)$  coherent states defined on the hyperboloid, commonly referred to as the  $SU(1,1)$  compass state [21], can also be represented on the stereographic (Poincaré disk) plane, which gives rise to  $SU(1,1)$ -based sub-Planck features.

The enhancement in sensitivity to phase-space displacements beyond the standard quantum limit (SQL) afforded by sub-Planck features depends on their structural form, with distinct behavior observed for anisotropic and isotropic configurations [16, 17, 35, 36]. Anisotropic sub-Planck structures yield direction-dependent enhancements in sensitivity to phase-space displacements, whereas isotropic counterparts exhibit a higher degree of sub-Planckness and enable phase-space sensitivity with greater precision [16]. These properties make isotropic sub-Planck features particularly attractive for quantum metrology. To the best of our knowledge, isotropic sub-Planck features within the  $SU(1,1)$  group have not yet been realized. In this work, we aim to develop refined sub-Planck features in the  $SU(1,1)$  framework by constructing multicomponent  $SU(1,1)$  compass states. Specifically, these generalized versions of the  $SU(1,1)$  compass state are constructed from the superposition of  $\bar{n}$  Perelomov  $SU(1,1)$  coherent states on the Poincaré disk, where  $\bar{n}$  ranges from small values ( $\bar{n} = 6$ ) to large values ( $\bar{n} \rightarrow \infty$ ). In these superpositions, the coherent states are symmetrically arranged along a circular path on the Poincaré disk, with the total number  $\bar{n}$  restricted to even values; each component state lies at the same distance from the origin, and adjacent states are separated by an angle of  $\frac{2\pi}{\bar{n}}$ . The resulting  $SU(1,1)$  compass states generate isotropic sub-Planck structures, and as the number of superposed coherent states increases, the isotropic nature of these features becomes more pronounced. Furthermore, our generalized  $SU(1,1)$  compass states exhibit isotropic enhancement in their sensitivity to phase-space displacements, resulting in precision that exceeds the SQL consistently across all displacement directions, making them valuable resources for quantum metrology applications.

\* [JiaXinPeng@ntu.edu.cn](mailto:JiaXinPeng@ntu.edu.cn)

† [dwang@ahu.edu.cn](mailto:dwang@ahu.edu.cn)

## II. THEORY

To make the discussion as self-contained as possible, we begin with a brief review of the main concepts underlying the present investigation, initially focusing on the role of phase-space characteristics of nonclassical states in quantum metrology. Nonclassical states play a crucial role in enhancing quantum metrological performance [37–42]. In more specific terms, the usefulness of a quantum state for these applications can be quantified by analyzing how distinguishable it becomes from its original form after a small perturbation [9], which reflects the sensitivity of the state to phase-space displacements and is closely related to the size of the smallest feature in the corresponding phase space. To understand this, let us consider the common example of the harmonic oscillator, where the system is governed by the annihilation operator  $\hat{a}$  and the creation operator  $\hat{a}^\dagger$ , which satisfy the canonical commutation relation  $[\hat{a}, \hat{a}^\dagger] = 1$ , with  $\hbar = 1$  hereafter. The Wigner function for a generic quantum state  $\hat{\rho}$  belonging to the HW group can be expressed as  $W_{\hat{\rho}}(\gamma) = \text{tr}[\hat{\rho}\hat{D}(\alpha)\hat{\Pi}\hat{D}^\dagger(\alpha)]$  with  $\hat{D}(\alpha) = \exp(\alpha\hat{a}^\dagger - \alpha^*\hat{a})$  being the displacement operator,  $\hat{\Pi} = (-1)^{\hat{a}^\dagger\hat{a}}$  denoting the parity operator, and  $\gamma = (x, p)^\top$  representing the position-momentum pair.

The overlap between a state and its slightly displaced version establishes a relationship between the state's sensitivity and the area of its smallest phase-space feature [9, 43]. This overlap for a generic state  $\hat{\rho}$  and its  $\delta$ -perturbed version can be expressed as  $S_{\hat{\rho}}(\delta) = \text{tr}[\hat{\rho}\hat{D}(\delta)\hat{D}^\dagger(\delta)]$ , which for any pure state  $|\psi\rangle$  takes the form  $S_{|\psi\rangle}(\delta) = |\langle\psi|\hat{D}(\delta)|\psi\rangle|^2$ , where  $|\psi'\rangle = \hat{D}(\delta)|\psi\rangle$  represents slightly displaced counterparts, with  $\delta = \delta x + i\delta p$  being the phase-space displacements. Alternatively, this overlap can be expressed in terms of corresponding Wigner functions [44], which relate the phase-space features via

$$S_{|\psi\rangle}(\delta) = \frac{2}{\pi} \int_{-\infty}^{\infty} dx dp W_{|\psi\rangle} W_{|\psi'\rangle}. \quad (1)$$

The phase-space area of a coherent state  $|\alpha\rangle$  adheres to the minimal uncertainty bound, with the overlap function given by  $S_{|\alpha\rangle}(\delta) = e^{-|\delta|^2}$ , for which distinguishability is achieved when  $|\delta| > 1$ , indicating that the coherent state is responsive to displacements at the SQL (shot noise limit), thereby setting its resolution as a metrological tool [10].

This led to the development of quantum states with finer phase-space features compared to coherent states, which may exhibit sensitivity greater than the SQL, often known as sub-shot noise sensitivity [9]. For instance, the HW macroscopic cat state, which is the superposition of two distinct coherent states ( $|\text{cat}\rangle \sim \left| \frac{x_0}{\sqrt{2}} \right\rangle + \left| -\frac{x_0}{\sqrt{2}} \right\rangle$  with  $x_0 \in \mathbb{R}$ ), may develop interference fringes that scale identically along the  $x$  direction but are finer than the coherent state along the  $p$  direction, with their extension

along  $p$  proportional to  $\frac{1}{x_0}$ , reaching a directional fineness in phase space. This scenario directly corresponds to phase-space sensitivity: a cat state with anisotropically finer phase-space features may also display an anisotropic enhancement in sensitivity compared to a coherent state [16]. The HW compass state ( $|\text{compass}\rangle \sim \left| \frac{x_0}{\sqrt{2}} \right\rangle + \left| -\frac{x_0}{\sqrt{2}} \right\rangle + \left| \frac{ix_0}{\sqrt{2}} \right\rangle + \left| -\frac{ix_0}{\sqrt{2}} \right\rangle$ ) exhibits sub-Planck features [4], which are phase-space features that are simultaneously localized along  $x$  and  $p$  directions, with a nearly uniform scaling of  $\frac{1}{x_0}$  [20]. This results in sensitivity enhancement dedicated to all phase-space directions, eventually providing greater sensitivity compared to the cat state. Subsequently, quantum states with finer sub-Planck features can reach better sensitivity than compass states [16, 35]. Similar sub-Planck features can also be achieved within the SU(1,1) group [45–48], highlighting an important symmetry relevant to quantum mechanics.

In the following, we employ the SU(1,1) quantum states to produce a refined version of sub-Planck features. The analysis is structured as follows: Sec. III covers the foundational concepts of the SU(1,1) group. Sec. IV highlights the main results, particularly the development of our SU(1,1) quantum states with exquisite sub-Planck features and their role in enhancing sensitivity to perturbation. Sec. V presents the generalization to higher-component superpositions and discusses the main features of our results, and Sec. VI summarizes the main findings of this work.

## III. GENERAL SETUP OF THE SU(1,1) GROUP

The irreducible representations of SU(1,1) are defined by the eigenvalues of the Casimir operator [45], namely

$$\hat{K}^2 = \hat{K}_0 - \frac{1}{2}(\hat{K}_+ \hat{K}_- + \hat{K}_- \hat{K}_+) = k(k-1)\mathbb{1} \quad (2)$$

with  $\hat{K}_+$ ,  $\hat{K}_-$ , and  $\hat{K}_0$  being the generators of the  $\mathfrak{su}(1,1)$  Lie algebra and satisfying the commutation relations  $[\hat{K}_0, \hat{K}_\pm] = \pm \hat{K}_\pm$ . Furthermore, the generators  $\hat{K}_\pm$  can be expressed in terms of the Hermitian operators  $\hat{K}_1$  and  $\hat{K}_2$  as  $\hat{K}_\pm = \pm i(\hat{K}_1 \pm i\hat{K}_2)$ . The action of the  $\mathfrak{su}(1,1)$  generators on the Fock space states  $\{|k, n\rangle; n \in \mathbb{N}\}$  is

$$\hat{K}_0 |k, n\rangle = (k+n) |k, n\rangle, \quad (3)$$

$$\hat{K}_+ |k, n\rangle = \sqrt{(n+1)(2k+n)} |k, n+1\rangle, \quad (4)$$

$$\hat{K}_- |k, n\rangle = \sqrt{n(2k+n+1)} |k, n-1\rangle, \quad (5)$$

where  $k$  is the Bargmann index, which is restricted to the positive discrete series.

The SU(1,1) displacement operator is expressed as [45]:

$$\begin{aligned} \hat{D}(\zeta) &= e^{\xi \hat{K}_+ - \xi^* \hat{K}_-}, \\ &= e^{\zeta \hat{K}_+} e^{\ln(1 - |\zeta|^2) \hat{K}_0} e^{-\zeta^* \hat{K}_-}, \end{aligned} \quad (6)$$

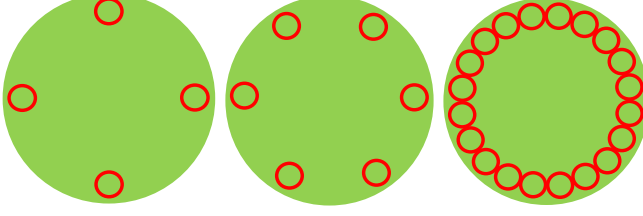


FIG. 1.  $SU(1,1)$  circular states are composed of  $\bar{n}$   $SU(1,1)$  coherent states (red circles) evenly distributed along a circular path in the Poincaré disk (the  $SU(1,1)$  phase space). We consider superpositions with  $\bar{n} > 4$ , restricted to even integers, where each adjacent component is separated by an equal angular spacing of  $\frac{2\pi}{\bar{n}}$ . In the limit  $\bar{n} \rightarrow \infty$ , the superposition approaches a continuous circular form.

where  $\xi = \frac{\tau}{2}e^{i\varphi}$  represents the points on the upper sheet of the two-sheet hyperboloid surface, and  $\zeta = e^{i\varphi} \tanh(\frac{\tau}{2})$ , where  $-\infty < \tau < \infty$  and  $0 < \varphi < 2\pi$ , which alternatively represents the stereographic projection of the upper sheet of the two-sheet hyperboloid onto the unit Poincaré disk with  $\zeta$  confined to  $0 \leq |\zeta| < 1$ .

The Premelov  $SU(1,1)$  coherent states are obtained by applying the displacement operator  $\hat{D}(\zeta)$  to the reference state  $|k, 0\rangle$  [33, 45], that is,

$$|\zeta, k\rangle = \hat{D}(\zeta) |k, 0\rangle. \quad (7)$$

Alternatively, the  $SU(1,1)$  coherent states can be associated with points on the two-sheeted hyperboloid surface, given by  $\mathbf{n} = (\cosh \tau, \sinh \tau \cos \varphi, \sinh \tau \sin \varphi)$ , representing the hyperbolic counterpart of the Bloch vector. The association between the  $SU(1,1)$  groups and the bosonic system belonging to the HW group can be established by the single- and two-mode bosonic realization of the  $SU(1,1)$  [49].

In the case of single-mode bosonic realization, corresponding generators can be expressed in terms of the creation ( $\hat{a}^\dagger$ ) and annihilation ( $\hat{a}$ ) operators as follows:

$$\hat{K}_+ = \frac{1}{2}\hat{a}^{\dagger 2}, \hat{K}_- = \frac{1}{2}\hat{a}^2, \hat{K}_0 = \frac{1}{4}(\hat{a}\hat{a}^\dagger + \hat{a}^\dagger\hat{a}). \quad (8)$$

The Casimir operator gets the form  $\hat{K}^2 = -\frac{3}{16}$ , which associates two Bargmann index ( $k$ ) values [49]. For  $k = \frac{1}{4}$ , the  $SU(1,1)$  coherent state leads to the typical squeezed vacuum state of the form given by

$$\left| \zeta, \frac{1}{4} \right\rangle = (1 - |\zeta|^2)^{\frac{1}{4}} \sum_{n=0}^{\infty} \frac{(2n!)^{\frac{1}{2}} \zeta^n}{2^n n!} |2n\rangle, \quad (9)$$

and  $k = \frac{3}{4}$  corresponds to

$$\left| \zeta, \frac{3}{4} \right\rangle = (1 - |\zeta|^2)^{\frac{3}{4}} \sum_{n=0}^{\infty} \frac{[(2n+1)!]^{\frac{1}{2}} \zeta^n}{2^n n!} |2n+1\rangle, \quad (10)$$

which represents the one-photon squeezed state [49, 50].

Let  $\hat{a}_1$  ( $\hat{a}_1^\dagger$ ) and  $\hat{a}_2$  ( $\hat{a}_2^\dagger$ ) be the annihilation (creation) operators for modes 1 and 2, respectively, and  $|n_1\rangle$  and  $|n_2\rangle$  denote the number state of these modes. The complete number-state basis for the two-mode field is denoted as  $|n_1, n_2\rangle = |n_1\rangle \otimes |n_2\rangle$ , and the corresponding generators get the following form:

$$\hat{K}_+ = \hat{a}_1^\dagger \hat{a}_2^\dagger, \hat{K}_- = \hat{a}_1 \hat{a}_2, \hat{K}_0 = \frac{1}{2}(\hat{a}_1^\dagger \hat{a}_1 + \hat{a}_2^\dagger \hat{a}_2 + 1). \quad (11)$$

Their action on  $|n_1, n_2\rangle$  satisfies

$$\hat{K}_0 |n_1, n_2\rangle = \frac{1}{2}(n_1 + n_2 + 1) |n_1, n_2\rangle, \quad (12)$$

$$\hat{K}_+ |n_1, n_2\rangle = \sqrt{(n_1 + 1)(n_2 + 1)} |n_1 + 1, n_2 + 1\rangle, \quad (13)$$

$$\hat{K}_- |n_1, n_2\rangle = \sqrt{n_1 n_2} |n_1 - 1, n_2 - 1\rangle. \quad (14)$$

The Casimir operator  $\hat{K}_0^2$  obeys  $\hat{K}_0^2 = \frac{1}{4}(\eta^2 - 1)$ , where  $\eta = \hat{a}_1^\dagger \hat{a}_1 - \hat{a}_2^\dagger \hat{a}_2$ , and its eigenvalue corresponds to the difference in the number of quanta between modes 1 and 2, i.e.,  $n_1 - n_2$ . The basis vector  $|k, n\rangle$  takes the form

$$k = \frac{1}{2}(\Delta + 1), n = \frac{1}{2}(n_1 + n_2 - \Delta), \quad (15)$$

where  $\Delta$  is the degeneracy parameter, representing the eigenvalue of  $|\eta|$ , which quantifies the asymmetry in the photon numbers between the two coupled modes. Consider a specific scenario when  $n_1 = n_2 + \Delta$  and  $n_2 = n = 0, 1, 2, \dots$ , implying that mode 1 has  $\Delta$  more photons than mode 2. The corresponding  $SU(1,1)$  Perelomov coherent states can be expressed in terms of the two-mode squeezed number states,

$$|\zeta, \Delta\rangle = (1 - |\zeta|^2)^{1+\Delta/2} \sum_{n=0}^{\infty} \sqrt{\frac{(n+\Delta)!}{n! \Delta!}} \zeta^n |n, n+\Delta\rangle, \quad (16)$$

which for  $\Delta = 0$  is the two-mode squeezed vacuum state [49].

#### IV. CIRCULAR $SU(1,1)$ SUPERPOSITIONS

The superposition of  $SU(1,1)$  coherent states can give rise to intriguing quantum states [21, 31]; however, surprisingly, such superpositions and their phase-space analysis have received little attention, particularly for cases involving a larger number of coherent states, which remain largely unexplored. Similar to the HW group [3], the  $SU(1,1)$  Wigner function can be expressed as the expectation value of the displaced parity operator [31, 32], denoted by

$$W_{\hat{\rho}}(\zeta) = \text{tr}[\hat{\rho} \hat{\Pi}(\zeta)], \quad (17)$$

where

$$\hat{\Pi}(\zeta) = \hat{D}(\zeta) \hat{\Pi} \hat{D}^\dagger(\zeta) \quad (18)$$

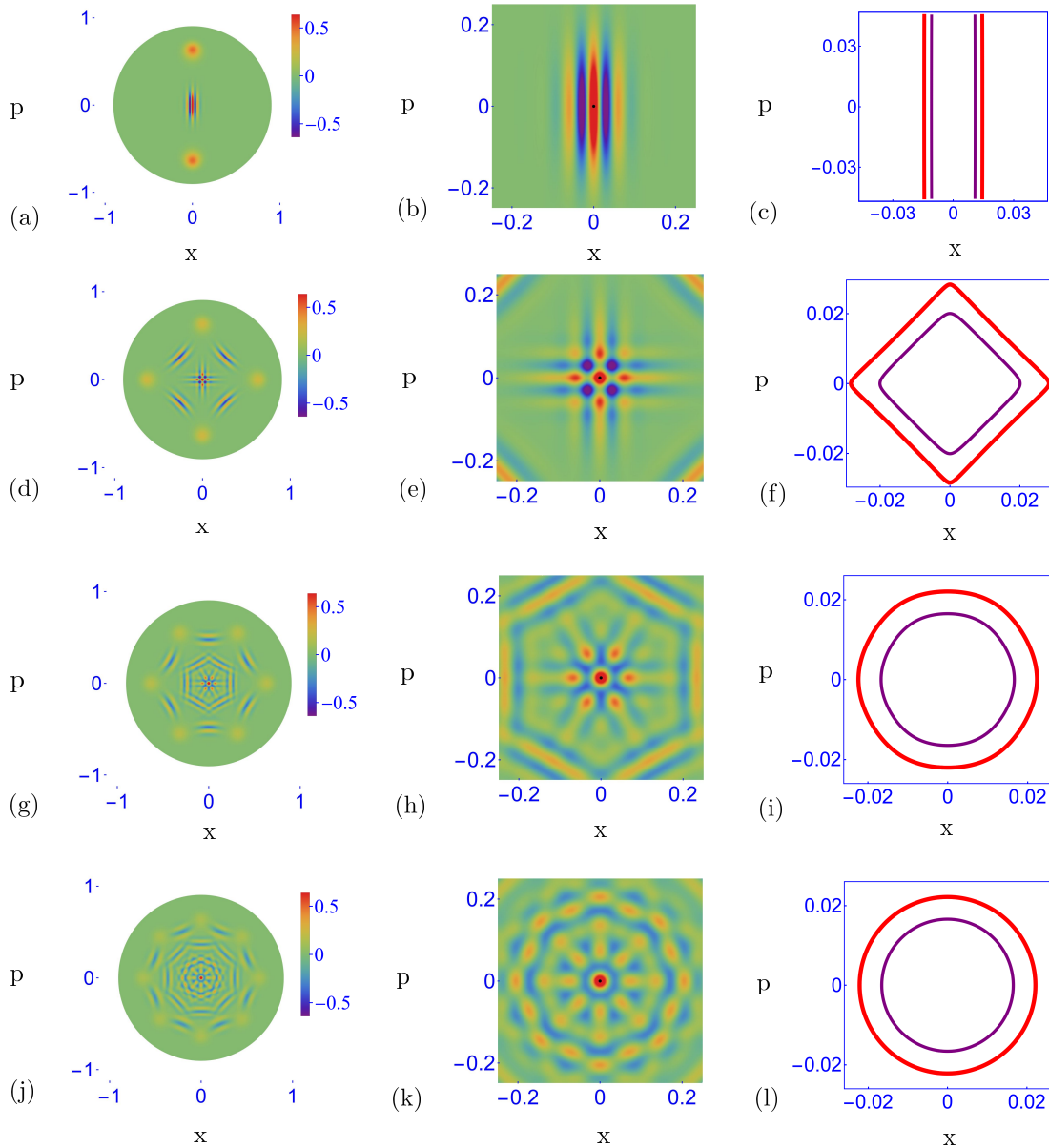


FIG. 2. The  $SU(1,1)$  Wigner distributions of our  $\bar{n}$ -component compass states are mapped onto the Poincaré disk for different values of  $\bar{n}$ , with each case containing a distinct central phase-space region highlighted by a black dot. (a)-(c) depict the  $SU(1,1)$  cat state: (a) displays the Wigner distribution, (b) highlights the central feature, and (c) displays the zeros associated with this central feature, with red and purple curves corresponding to  $k = 12$  and  $k = 16$ , respectively. (d)-(f) represent the case when  $\bar{n} = 4$ , it is the  $SU(1,1)$  compass state, where its Wigner distribution is shown in (d), its central feature in (e), and the zeros associated with this feature in (f), again with red and purple curves corresponding to  $k = 12$  and  $k = 16$ , respectively. The case  $\bar{n} = 6$  is presented in (g)-(i), where (g) shows the Wigner distribution, (h) emphasizes the central feature, and (i) depicts the zeros corresponding to this feature (red curve for  $k = 12$ , purple curve for  $k = 16$ ). Finally, for  $\bar{n} = 8$  (j)-(l), (j) shows the Wigner distribution, (k) the central feature, and (l) the zeros associated with it for  $k = 12$  (red curve) and  $k = 16$  (purple curve). In all cases,  $\bar{\tau} = 1.5$ .

with  $\hat{\Pi} = e^{i\pi(\hat{K}_0 - k)}$  is the displaced parity operator. For a generic  $SU(1,1)$  operator  $\hat{\rho} = |\zeta_i\rangle\langle\zeta_j|$ , this leads to

$$W_{|\zeta_i\rangle\langle\zeta_j|}(\zeta) = \exp\left[2i\text{arg}\left(\frac{A}{B}\right)\right] \left\langle \frac{\zeta_j - \zeta}{A} \right| \hat{\Pi} \left| \frac{\zeta_i - \zeta}{B} \right\rangle, \quad (19)$$

where  $A = 1 - \zeta_j\zeta^*$  and  $B = 1 - \zeta_i\zeta^*$ , which in the case of the  $SU(1,1)$  coherent state  $|k, 0\rangle$  gets the form

$$W_{|k, 0\rangle}(\zeta) = \sqrt{\left(\frac{|\zeta|^2 - 1}{|\zeta|^2 + 1}\right)^{4k}} \simeq e^{-4k|\zeta|^2} \text{ for } k \gg 1. \quad (20)$$

This suggests that the spatial extension of the  $SU(1,1)$  coherent state along any direction in phase space is proportional to  $\frac{1}{\sqrt{k}}$ .

Refined sub-Planck features of the HW group have been realized through establishing multicomponent cat states [16]. Extending these concepts to the  $SU(1,1)$  group can be challenging due to the mathematical complexities associated with  $SU(1,1)$ . To achieve this, we consider superpositions of  $SU(1,1)$  coherent states, which are arranged in a specific configuration on the Poincaré disk, as illustrated in Fig. 1. These superposed components form a circular pattern on the Poincaré disk for higher values of  $\bar{n}$ , which can be mathematically expressed as follows:

$$|\bigcirc_{\bar{n}}\rangle = \sum_{j=0}^{\bar{n}-1} \left| e^{2\pi i j/\bar{n}} \tanh\left(\frac{\bar{\tau}}{2}\right) \right\rangle \quad (21)$$

with  $\bar{\tau}$  kept constant throughout. The Wigner function of these superpositions is obtained by using Eq. (19), which is solely influenced by  $k$  and mathematically denoted as,

$$W_{|\bigcirc_{\bar{n}}\rangle}(\zeta) = \sum_{i,j=0}^{\bar{n}-1} W_{|\zeta_i\rangle\langle\zeta_j|}(\zeta), \quad \text{where } \zeta = x + ip. \quad (22)$$

Note that, where  $x$  and  $p$  notations should not mix with the position-momentum quadratures; here they refer to the stereographic projection. Different values of  $\bar{n}$  correspond to different superpositions, each with distinct phase-space features, as discussed below.

### A. Anisotropy-driven improvements

Let us start when  $\bar{n} = 2$  in Eq. (21), representing the  $SU(1,1)$  cat state [21, 31], whose associated Wigner function [Eq. (22)] is illustrated on the Poincaré disk ( $SU(1,1)$  phase space), see Figs. 2(a)-2(c). Fig. 2(a) represents the Wigner distribution of the  $SU(1,1)$  cat state, with interference fringes appearing around the phase-space origin, which are further emphasized in Fig. 2(b). Fig. 2(c) represents the boundary of the central patch (marked by a black dot in Fig. 2(b)), specifically obtained by approximating zeros of the central patch under variable values of  $k$ . Here, lower (red) to higher  $k$  (purple) indicates an inverse relationship between  $k$  and the extension of the feature [21]. This depiction also clearly outlines the edges of the feature. It has been noted that this highlighted central feature has the same extension along  $p$  as those of the coherent state (extension along  $p$  is proportional to  $\frac{1}{\sqrt{k}}$ ), but is more shrunk by a factor of  $\frac{1}{\sqrt{k}}$  along  $x$  than that of the coherent state, suggesting greater refinement along a single direction in phase space when compared to the coherent state [21].

When  $\bar{n} = 4$  in Eq. (21), it results in the  $SU(1,1)$  compass state [21], consisting of four coherent states, which

are equidistant from the origin and uniformly placed on the Poincaré disk. The corresponding Wigner function of this compass state can be obtained from Eq. (22), which is illustrated in Fig. 2(d). Apparently this Wigner distribution adopts a tilted square-like shape on the Poincaré disk, with a variety of phase-space features contained inside it, such as the yellow lobes at the corners representing the component coherent states. Between each component state, cat-like interference fringes emerge, creating a striking billboard-like pattern around the origin of the Poincaré disk. This central pattern is further shown in Fig. 2(e), where a single tile, marked with a black dot, is selected for further illustration. In Fig. 2(f), we plot the zero-amplitude points of the central tile for different values of  $k$ , effectively highlighting the regions where it is confined. This central tile reflects the main sub-Planck feature of the  $SU(1,1)$  compass state. Its phase-space extension is roughly proportional to  $\frac{1}{k}$  in any direction, exhibiting a greater phase-space resolution than cat states. Transitioning from cat to compass states results in a finer phase-space feature, but as emphasized in Fig. 2(f), this resultant central sub-Planck feature still exhibits notable anisotropy, and this anisotropy continues as the state parameters change, especially with different  $k$  values, as shown by the shift from red to purple curves in Fig. 2(f). Such an anisotropic nature of sub-Planck features may put limits on their application in quantum measurements.

### B. Improved directional uniformity in phase space

We now examine superpositions involving a larger number of coherent states  $\bar{n}$  in Eq. (21), focusing on the cases  $\bar{n} = 6$  and  $\bar{n} = 8$ . Generalizations to  $\bar{n} = 10$ ,  $\bar{n} = 12$ , and  $\bar{n} = 16$  are discussed subsequently. Setting  $\bar{n} = 6$  in Eq. (21) results in a six-component compass state, and its associated Wigner function can be obtained by setting  $\bar{n} = 6$  in Eq. (22), which is depicted on the Poincaré disk, as shown in Fig. 2(g), where component coherent states are clearly apparent (yellowish lobes), with cat-like interference fringes and a kaleidoscopic-like pattern appearing around the origin, where outer features of this distribution give the impression of a hexagon on the Poincaré disk. In Fig. 2(h), the central portion of the Poincaré disk is emphasized, where the feature of interest is highlighted with a black dot. Fig. 2(i) highlights the boundary of the central feature, which is obtained by approximating its associated zero-amplitude regions, displaying a nearly circular shape that becomes more localized as  $k$  increases (as demonstrated in the red-to-purple curves of Fig. 2(i)). This evidences the shape of the central feature being nearly isotropic in phase space, with its extension being inversely proportional to  $k$  in all directions of phase space.

When comparing the central sub-Planck feature of the six-component compass state illustrated in Fig. 2(i) with that of the compass state shown in Fig. 2(f),

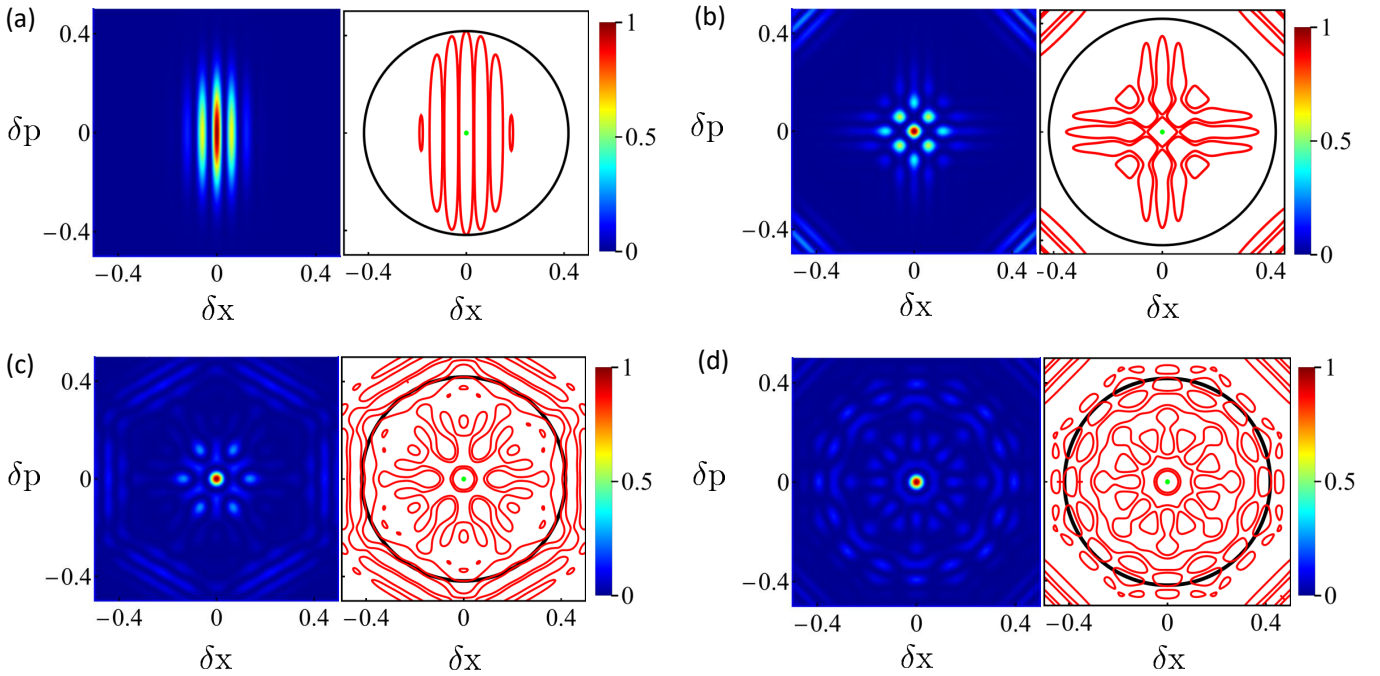


FIG. 3. The left panels show the overlap  $S_{|\bigcirc_{\bar{n}}\rangle}(\delta)$  with  $\delta = \delta x + i\delta p$ , where the corresponding zeros are illustrated in the right panels of each image. (a)  $\bar{n} = 2$ ; (b)  $\bar{n} = 4$ ; (c)  $\bar{n} = 6$ ; (d)  $\bar{n} = 8$ . In all exhibited scenarios,  $\bar{\tau} = 1.5$ .

greater isotropy is associated with the feature of the six-component compass state, indicating a notable improvement in sub-Planckness towards higher-component compass states. Note that the isotropic, localized features that simultaneously localize in all directions of phase space are more in line with the definition of the sub-Planck feature. This can be succinctly described as a higher level of sub-Planckness being attained compared to the compass state.

Setting  $\bar{n} = 8$  in Eq. (21) leads to a superposition of eight coherent states, establishing our eight-component compass state. The Wigner function of this compass state can be derived by substituting  $\bar{n} = 8$  into Eq. (22). We illustrate corresponding Wigner distribution in Fig. 2(j), with its central portion is illustrated in Figs. 2(k) and 2(l). As depicted in Fig. 2(j), this Wigner function reveals more pronounced phase-space features: this particular arrangement of coherent states develops an octagon-like shape consisting of cat-like interference fringes between the component states, along with a pronounced kaleidoscopic pattern appears around the origin of the Poincaré disk, which is further highlighted in Fig. 2(k), with the feature of interest marked by a black dot existing at the center of the pattern. A deeper investigation of this feature is conducted to determine its boundary and confirm its shape by identifying the region where it diminishes, as shown in Fig. 2(l). This analysis reveals that the feature has a perfect circular shape, with a noticeable improvement compared to the previous cases of four- and six-component compass states. For higher values of  $k$  (represented by the red

and purple curves in Fig. 2(l)), the feature becomes more tightly confined within the circular region. This trend of enhanced sub-Planck resolution, demonstrated by the emergence of a circularly localized sub-Planck feature, is preserved in higher-component superpositions, such as the ten- ( $\bar{n} = 10$ ), twelve- states  $\bar{n} = 12$ , and sixteen-component compass states  $\bar{n} = 16$ , which are detailed in the subsequent discussion. The sensitivity of a state to displacements, arising from its sub-Planck features, can be quantified by examining its orthogonality under infinitesimal shifts [9]; this approach is extended below for our  $SU(1,1)$  superpositions.

### C. Displacement sensitivity and future prospects

The overlap between a state and its slightly displaced versions analyzes a state's response to displacements and eventually characterizes sensitivity. Specifically, the overlap  $S_{|\bigcirc_{\bar{n}}\rangle}(\delta) = |\langle \bigcirc_{\bar{n}} | \hat{D}(\delta) | \bigcirc_{\bar{n}} \rangle|^2$ , which can also be related to the corresponding Wigner phase space using Eq. (1), and its associated orthogonality  $S_{|\bigcirc_{\bar{n}}\rangle}(\delta) \simeq 0$ , reflects the state's response to displacement (sensitivity to phase-space displacements). In our case, this overlap reads

$$S_{|\bigcirc_{\bar{n}}\rangle}(\delta) = \left| \sum_{i,j=0}^{\bar{n}-1} S_{|\zeta_i\rangle\langle\zeta_j|}(\delta) \right|^2 \quad (23)$$

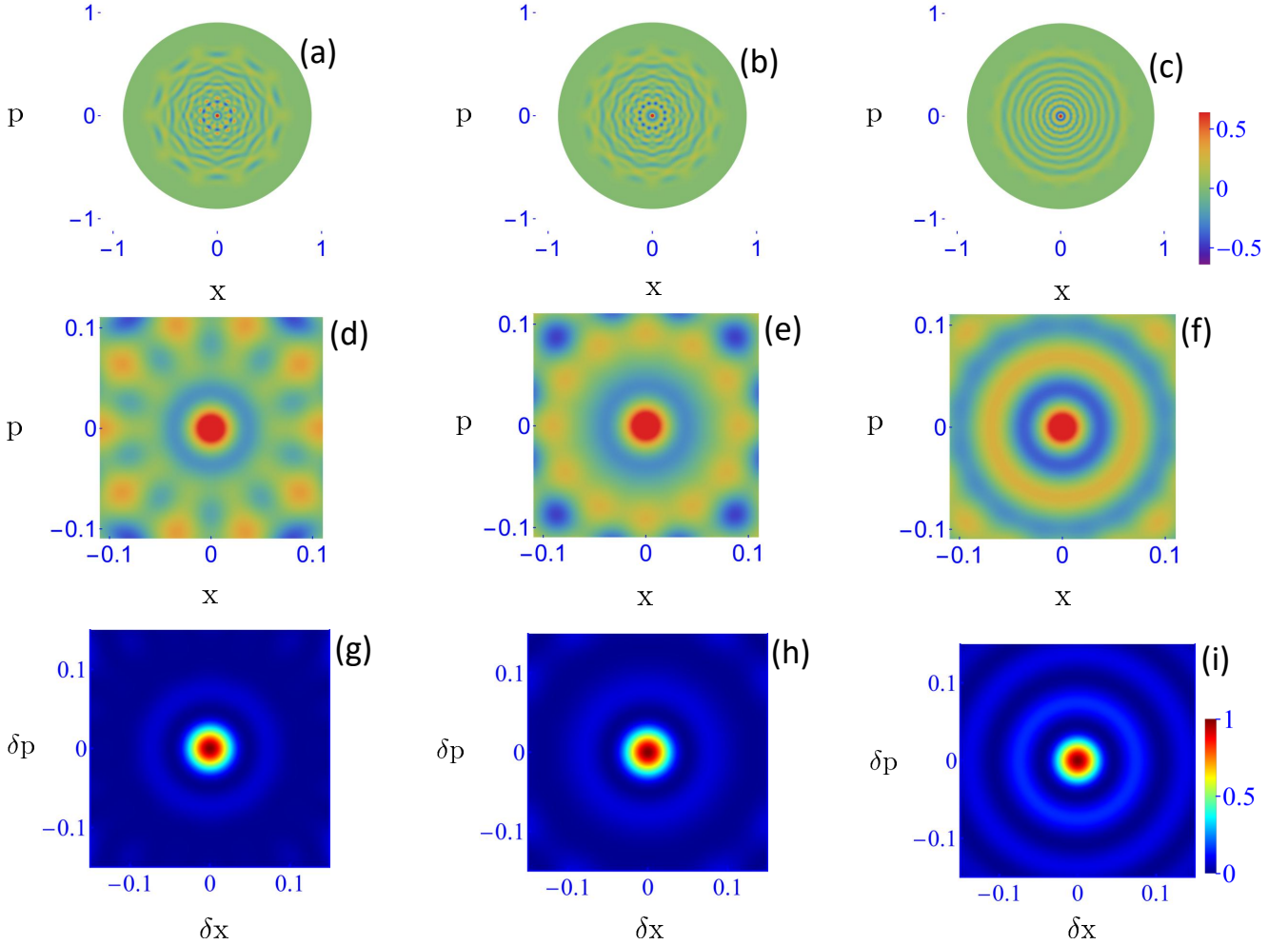


FIG. 4. The SU(1,1) Wigner distribution and their associated overlaps for  $\bar{n}$  component SU(1,1) superpositions of the present work: (a) Wigner distribution for  $\bar{n} = 10$ , with its central close-up in (d) and associated overlap in (g); (b) Wigner distribution for  $\bar{n} = 12$ , with its central close-up in (e) and associated overlap in (h); and (c) Wigner distribution for  $\bar{n} = 16$ , with its central close-up in (f) and associated overlap in (i). In all cases,  $\bar{\tau} = 1.5$ .

with

$$S_{|\zeta_i\rangle\langle\zeta_j|}(\delta) = e^{-2ik\arg(1+\delta^*\zeta_j)} \left[ \frac{(1-|\zeta_i|^2)(1-\left|\frac{\delta+\zeta_j}{1+\delta^*\zeta_j}\right|^2)^k}{(1-\zeta_i^*)(\frac{\delta+\zeta_j}{1+\delta^*\zeta_j})} \right]. \quad (24)$$

Fig. 3 illustrates the corresponding overlap  $S_{|\bigcirc_{\bar{n}}\rangle}(\delta)$  for the SU(1,1) quantum states of interest, extending the discussion from well-known states to more complex, multicomponent superpositions explored in this work. The overlap function between the SU(1,1) coherent state  $|0, k\rangle$  and its displaced version  $\hat{D}(\delta)|0, k\rangle$  is given by  $S_{|0,k\rangle}(\delta) = e^{-k|\delta|^2}$ , with its vanishing regions represented by a black circle, which appears alongside each illustration in Fig. 3. The extension of this circle is proportional to  $\frac{1}{\sqrt{k}}$ , which measures the amount of displacement required for the SU(1,1) coherent to achieve orthogonality and predicts the sensitivity of SU(1,1) coherent states. This can be

considered as the minimum norm (or SQL), against which the sensitivity of each state is compared.

We now examine the overlap function  $S_{|\bigcirc_{\bar{n}}\rangle}(\delta)$  for multiple  $\bar{n}$  values associating our SU(1,1) superpositions. Starting with the overlap function of the previously identified SU(1,1) cat state ( $\bar{n} = 2$ ) [21], shown in Fig. 3(a) (left panel), we illustrate its vanishing regions in Fig. 3(a) (right panel). The central feature in Fig. 3(a) (right panel), marked by the green dot, illustrates that along the  $p$ -direction in phase space, a displacement  $\delta x \simeq \frac{1}{k}$  (which is  $\frac{1}{\sqrt{k}}$  smaller than that of coherent state) can make the SU(1,1) cat state orthogonal to its  $\delta$ -perturbed version. In contrast, along the  $p$ -direction, a displacement  $\delta p$ , of the same order as that of a coherent state (as observed in the central feature of the right panel of Fig. 3(a), where the central feature marked by the green dot coincides with the level of the coherent states) reaches distinguishability for a displacement proportional to  $\frac{1}{\sqrt{k}}$ .

This demonstrates that the cat state is responsive to displacements smaller than the SQL along a specific direction, achieving an anisotropic enhancement in sensitivity.

The case with  $\bar{n} = 4$  in Eq. (23) determines the sensitivity of the  $SU(1,1)$  compass state, as shown in Fig. 3(b). Similar descriptions apply to the  $SU(1,1)$  compass state, which we summarize here: When compared to the  $SU(1,1)$  cat state, the overlap of the compass state can attain orthogonality for displacements  $\delta \simeq \frac{1}{k}$  along any arbitrary direction in phase space. This suggests directional independence in sensitivity enhancement, providing advantages over cat states. However, as observed, the distinguishability occur in tile-like regions (see the central region of Fig. 3(b) in the right panel, which is marked with a green dot) reveals the nonuniformity of displacements causing orthogonality of the state. This indicates the imperfections associated with state's sensitivity in detecting such minor displacements, as the behavior is not perfectly isotropic. Some directions offer more resolution than others.

We observe that the anisotropic imperfections in the sensitivity of the  $SU(1,1)$  compass state can be progressively corrected by incorporating more components of coherent states in our superpositions, ultimately leading to perfect isotropic sensitivity enhancement and making them more desirable than their lower-order counterparts. For  $\bar{n} = 6$  in Eq. (23), indicating the overlap between a six-component compass state and its displaced version, as depicted in Fig. 3(c), where the left panel represents the overlap function and its associated zero-amplitude regions are shown in the right panel, evidencing orthogonality at much smaller displacement compared to the coherent state. Notably, this distinguishability is achieved for displacement proportional to  $\frac{1}{k}$ , occurring in a more isotropic manner compared to the compass state, as evidenced by the circular region marked with a green dot in Fig. 3(c) (right panel). Our eight-component compass state achieved enhanced sensitivity to displacement compared to its  $\bar{n} \leq 6$  counterparts. As shown in Fig. 3(d), the overlap and its associated orthogonality are concentrated in a more tightly confined isotropic region, represented by the green-dotted circular area. This indicates that a superposition of eight coherent states provides a greater isotropic improvement in displacement sensitivity compared to the lower-order superpositions examined in this study. Extending these superpositions to higher  $\bar{n}$  values preserves this enhanced sensitivity with even greater precision.

Quantum states with fine-scale phase-space features can provide significant advantages in quantum metrology [9–13]. In this context, our higher-component  $SU(1,1)$  compass states, exhibiting refined sub-Planck structures, hold significant potential. Notably, these advanced  $SU(1,1)$  sub-Planckian features appear to differ from their earlier HW counterparts [16], especially in their construction. The potential applications of these sub-Planckian features may extend beyond those of the HW counterparts.

## V. GENERALIZATION AND OUTLOOK

We now generalize our results for higher values of  $\bar{n}$ , including  $\bar{n} = 10, 12$ , and  $16$ . As we observed, increasing the number of  $SU(1,1)$  coherent states in our superpositions enhances the isotropic nature of the sub-Planck traits, which is also sustained by our higher-component compass states, as depicted in Figs. 4(a) for  $\bar{n} = 10$ , 4(b) for  $\bar{n} = 12$ , and 4(c) for  $\bar{n} = 16$ , along with their central features highlighted in Figs. 4(d), 4(e), and 4(f). In these superpositions, an isotropic feature develop at the center of the Poincaré disk. Our illustrations include the superposition of up to  $\bar{n} = 16$   $SU(1,1)$  coherent states. The Wigner distribution is shown in Fig. 4(c), and the corresponding close-up in Fig. 4(f) highlights the isotropic sub-Planck feature at the center of the Poincaré disk. While these illustrations can be further extended, we did not find it necessary, as the general trend of the superpositions has already been conveyed. This suggests that the isotropic characteristics will be preserved for higher component superpositions with increased improvements. Moreover, the overlaps corresponding to these superpositions, shown in Figs. 4(g) for  $\bar{n} = 10$ , 4(h) for  $\bar{n} = 12$ , and 4(i) for  $\bar{n} = 16$ , indicate an isotropic response to phase-space displacements, suggesting a uniform enhancement in sensitivity.

Our isotropic sub-Planck features holds symmetric extension proportional to  $\frac{1}{k}$  along all phase-space directions, which for considerably large  $k$  values ( $k \gg 1$ ) is significantly smaller than that of a coherent state ( $SU(1,1)$  sub-Planck structure). Under these conditions the  $SU(1,1)$  coherent state may lead to two-mode squeezed number states  $|\zeta, \Delta\rangle$ , as demonstrated in Eq. (16). This shows that our superposition under this limit can be regarded as the superposition of two-mode squeezed number states; specifically, in this case, the Bargmann index  $k$  is proportional to  $\Delta$  (i.e.,  $k \propto \Delta$ ), where  $\Delta$  represents the photon number asymmetry between the two correlated modes of the two-mode squeezed number states. Higher  $k$  causes greater asymmetry in the photon number of two coupled modes of the two-mode squeezed number states. In other words, this increased asymmetry favors the formation of sub-Planck features in our instances.

## VI. SUMMARY

In summary, we have proposed superpositions involving  $\bar{n}$  number of  $SU(1,1)$  coherent states ( $\bar{n}$ -component  $SU(1,1)$  compass states) to generate an improved version of sub-Planck features. These resultant sub-Planck features outperform their previously established counterparts [21]. Specifically, the superposition involving  $\bar{n} \geq 6$  coherent states (with the total number limited to even integers), which are uniformly distributed around the Poincaré disk; that is, each coherent state exhibits the same distance from the phase-space origin, and adjacent components separated by a uniform an-

gular spacing of  $\frac{2\pi}{\bar{n}}$ , develops the isotropic sub-Planck traits. The isotropic nature of the resulting sub-Planck feature improves as the number of coherent states in the superpositions grows. We examined the superposition up to sixteen  $SU(1,1)$  coherent states ( $\bar{n} = 16$ ), which can be generalized for bigger  $\bar{n}$  (possibly  $\bar{n} \rightarrow \infty$ ). These higher-order superpositions, with their refined sub-Planck phase-space features, reach isotropic enhancement in sensitivity to displacement, highlighting their significance for quantum metrology.

## ACKNOWLEDGEMENT

This work was supported by the National Natural Science Foundation of China (Grants No. 12475009, and No. 12075001), the Anhui Province Science and Technology Innovation Project (Grant No. 202423r06050004), the Anhui Provincial Department of Industry and Information Technology (Grant No. JB24044), the Anhui Province Natural Science Foundation (Grant No. 202508140141), and the Anhui Provincial University Scientific Research Major Project (Grant No. 2024AH040008). Jia-Xin Peng acknowledges the support from the National Natural Science Foundation of China (Grant No. 12504566), the Natural Science Foundation of Jiangsu Province (Grant No. BK20250947), the Natural Science Foundation of the Jiangsu Higher Education Institutions (Grant No. 25KJB140013), and the Natural Science Foundation of Nantong City (Grant No. JC2024045).

---

[1] H. P. Robertson, The uncertainty principle, *Phys. Rev.* **34**, 163 (1929).

[2] J. A. Wheeler and W. H. Zurek, *Quantum Theory and Measurement* (Princeton University Press, Princeton, NJ, 1983).

[3] W. P. Schleich, *Quantum Optics in Phase Space* (Wiley-VCH, Weinheim, 2001).

[4] W. H. Zurek, Sub-Planck structure in phase space and its relevance for quantum decoherence, *Nature* **412**, 712 (2001).

[5] L. Praxmeyer, P. Wasylczyk, C. Radzewicz, and K. Wódkiewicz, Time-frequency domain analogues of phase space sub-Planck structures, *Phys. Rev. Lett.* **98**, 063901 (2007).

[6] L. A. Howard, T. J. Weinhold, F. Shahandeh, J. Combes, M. R. Vanner, A. G. White, and M. Ringbauer, Quantum hypercube states, *Phys. Rev. Lett.* **123**, 020402 (2019).

[7] P. Jacquod, I. Adagideli, and C. W. J. Beenakker, Decay of the Loschmidt echo for quantum states with sub-Planck-scale structures, *Phys. Rev. Lett.* **89**, 154103 (2002).

[8] W. H. Zurek, Decoherence, einselection, and the quantum origins of the classical, *Rev. Mod. Phys.* **75**, 715 (2003).

[9] F. Toscano, D. A. R. Dalvit, L. Davidovich, and W. H. Zurek, Sub-Planck phase-space structures and Heisenberg-limited measurements, *Phys. Rev. A* **73**, 023803 (2006).

[10] D. A. R. Dalvit, R. L. de Matos Filho, and F. Toscano, Quantum metrology at the Heisenberg limit with ion trap motional compass states, *New J. Phys.* **8**, 276 (2006).

[11] P. Zheng, Y. Cai, B. Xu, S. Wen, L. Zhang, Z. Ni, J. Mai, Y. Zeng, L. Lin, L. Hu, X. Deng, S. Liu, J. Shu, Y. Xu, and D. Yu, Quantum-enhanced dark matter detection using Schrödinger cat states (2025), [arXiv:2507.23538 \[quant-ph\]](https://arxiv.org/abs/2507.23538).

[12] X. Deng, S. Li, Z.-J. Chen, Z. Ni, Y. Cai, J. Mai, L. Zhang, P. Zheng, H. Yu, C.-L. Zou, and et al., Quantum-enhanced metrology with large Fock states, *Nat. Phys.* **20**, 1874–1880 (2024).

[13] L. Praxmeyer, C.-C. Chen, P. Yang, S.-D. Yang, and R.-K. Lee, Direct measurement of time-frequency analogs of sub-Planck structures, *Phys. Rev. A* **93**, 053835 (2016).

[14] Arman and P. K. Panigrahi, Generating overlap between compass states and squeezed, displaced, or Fock states, *Phys. Rev. A* **109**, 033724 (2024).

[15] Arman and P. K. Panigrahi, Enhancing the size of phase-space states containing sub-Planck-scale structures via non-Gaussian operations (2026), [arXiv:2601.15654 \[quant-ph\]](https://arxiv.org/abs/2601.15654).

[16] T. Hailin, N. Akhtar, and G. Xianlong, Multicomponent cat states with sub-Planckian structures and their optomechanical analogues, *Phys. Rev. Appl.* **24**, 024053 (2025).

[17] S. Tang, S. Luo, and Y. Zhang, Sub-Planck structures and phase-space sensitivity of circular states, *Phys. Rev. A* **112**, 023712 (2025).

[18] N. Akhtar, J. Wu, J.-X. Peng, W.-M. Liu, and G. Xianlong, Sub-Planck structures and sensitivity of the superposed photon-added or photon-subtracted squeezed-vacuum states, *Phys. Rev. A* **107**, 052614 (2023).

[19] D. W. Moore, V. Švarc, K. Singh, A. Kovalenko, M. T. Pham, O. Číp, L. Slodička, and R. Filip, Sub-Planck structure quantification in non-Gaussian probability densities (2026), [arXiv:2601.05898 \[quant-ph\]](https://arxiv.org/abs/2601.05898).

[20] N. Akhtar, B. C. Sanders, and C. Navarrete-Benlloch, Sub-Planck structures: Analogies between the Heisenberg-Weyl and  $SU(2)$  groups, *Phys. Rev. A* **103**, 053711 (2021).

[21] N. Akhtar, B. C. Sanders, and G. Xianlong, Sub-Planck phase-space structure and sensitivity for  $SU(1,1)$  compass states, *Phys. Rev. A* **106**, 043704 (2022).

[22] W. Du, J. F. Chen, Z. Y. Ou, and W. Zhang, Quantum dense metrology by an  $SU(2)$ -in- $SU(1,1)$  nested interferometer, *Appl. Phys. Lett.* **117**, 024003 (2020).

[23] M. Liu, H. Miao, and L. Zhang, Realizing the optimal measurement scheme for an  $SU(1,1)$  interferometer in ab initio phase estimation, *Phys. Rev. A* **111**, 063711 (2025).

- [24] F. Hudelist, J. Kong, C. Liu, J. Jing, Z. Ou, and W. Zhang, Quantum metrology with parametric amplifier-based photon correlation interferometers, *Nat. Commun.* **5**, 1 (2014).
- [25] K. Berrada, Quantum metrology with  $SU(1,1)$  coherent states in the presence of nonlinear phase shifts, *Phys. Rev. A* **88**, 013817 (2013).
- [26] S. S. Szigeti, R. J. Lewis-Swan, and S. A. Haine, Pumped-up  $SU(1,1)$  interferometry, *Phys. Rev. Lett.* **118**, 150401 (2017).
- [27] H. Liang, Y. Su, X. Xiao, Y. Che, B. C. Sanders, and X. Wang, Criticality in two-mode interferometers, *Phys. Rev. A* **102**, 013722 (2020).
- [28] D. Linnemann, J. Schulz, W. Muessel, P. Kunkel, M. Prüfer, A. Frölian, H. Strobel, and M. K. Oberthaler, Active  $SU(1,1)$  atom interferometry, *Quantum Sci. Technol.* **2**, 044009 (2017).
- [29] G. S. Agarwal, Saturation of the quantum Cramér-Rao bound for distributed sensing via error sensitivity in  $SU(1,1)$ - $SU(m)$  interferometry, *Phys. Rev. A* **112**, 032439 (2025).
- [30] P. G. Morrison, Matrix Wigner function and  $SU(1,1)$  (2023), [arXiv:2306.01238 \[quant-ph\]](https://arxiv.org/abs/2306.01238).
- [31] A. B. Klimov, U. Seyfarth, H. de Guise, and L. L. Sánchez-Soto,  $SU(1, 1)$  covariant s-parametrized maps, *J. Phys. A: Math. Theor.* **54**, 065301 (2021).
- [32] U. Seyfarth, A. B. Klimov, H. d. Guise, G. Leuchs, and L. L. Sanchez-Soto, Wigner function for  $SU(1,1)$ , *Quantum* **4**, 317 (2020).
- [33] C. C. Gerry, Correlated two-mode  $SU(1,1)$  coherent states: nonclassical properties, *J. Opt. Soc. Am. B* **8**, 685 (1991).
- [34] C. C. Gerry and R. Grobe, Two-mode intelligent  $SU(1,1)$  states, *Phys. Rev. A* **51**, 4123 (1995).
- [35] N. Akhtar, X. Yang, J.-X. Peng, I. Ul Haq, Y. Xie, and Y. Chen, Sub-shot-noise sensitivity via superpositions of two deformed kitten states, *Phys. Rev. A* **111**, 032407 (2025).
- [36] A. Shukla and B. C. Sanders, Superposing compass states for asymptotic isotropic sub-Planck phase-space sensitivity, *Phys. Rev. A* **108**, 043719 (2023).
- [37] A. Sinatra, Spin-squeezed states for metrology, *Appl. Phys. Lett.* **120**, 120501 (2022).
- [38] J. Czartowski, K. Życzkowski, and D. Braun, Minimal-noise estimation of noncommuting rotations of a spin, *Quantum* **8**, 1341 (2024).
- [39] J. Martin, S. Weigert, and O. Giraud, Optimal detection of rotations about unknown axes by coherent and anticoherent states, *Quantum* **4**, 285 (2020).
- [40] L. Pezzè, A. Smerzi, M. K. Oberthaler, R. Schmied, and P. Treutlein, Quantum metrology with nonclassical states of atomic ensembles, *Rev. Mod. Phys.* **90**, 035005 (2018).
- [41] K. Xu, Y.-R. Zhang, Z.-H. Sun, H. Li, P. Song, Z. Xiang, K. Huang, H. Li, Y.-H. Shi, C.-T. Chen, X. Song, D. Zheng, F. Nori, H. Wang, and H. Fan, Metrological characterization of non-gaussian entangled states of superconducting qubits, *Phys. Rev. Lett.* **128**, 150501 (2022).
- [42] P. T. Gochowski and R. Filip, Optimal phase-insensitive force sensing with non-Gaussian states, *Phys. Rev. Lett.* **135**, 230802 (2025).
- [43] K. M. R. Audenaert, Comparisons between quantum state distinguishability measures, *Quantum Inf. Comput.* **14**, 31 (2014).
- [44] D. Alonso, S. Brouard, J. P. Palao, and R. S. Mayato, Action scales for quantum decoherence and their relation to structures in phase space, *Phys. Rev. A* **69**, 052111 (2004).
- [45] A. Perelomov, *Generalized Coherent States and Their Applications*, Theoretical and Mathematical Physics (Springer-Verlag, Berlin, 1986).
- [46] K. Berrada, Quantum metrology with  $SU(1,1)$  coherent states in the presence of nonlinear phase shifts, *Phys. Rev. A* **88**, 013817 (2013).
- [47] J. Ma, X. Wang, C.-P. Sun, and F. Nori, Quantum spin squeezing, *Phys. Rep.* **509**, 89 (2011).
- [48] Z. Shaterzadeh-Yazdi, P. S. Turner, and B. C. Sanders,  $SU(1,1)$  symmetry of multimode squeezed states, *J. Phys. A: Math. Theor.* **41**, 055309 (2008).
- [49] C. C. Gerry, Remarks on the use of group theory in quantum optics, *Opt. Express* **8**, 76 (2001).
- [50] C. F. Lo, Normal ordering of the  $SU(1,1)$  and  $SU(2)$  squeeze operators, *Phys. Rev. A* **51**, 1706 (1995).